sciendo

Nordic Concrete Federation

ISSN online 2545-2819
ISSN print 0800-6377

DOI: 10.2478/ncr-2024-0006

Received: April 2, 2024
Revision received: June 21, 2024
Accepted: June 24, 2024

Determining the Influence of Curing Temperature and SCMs on C-A-S-H Composition Using SEM-EDS Hypermaps

Petter Hemstad, Dr.
Project manager
Heidelberg Materials Sement Norge AS
Setrevegen 2
3950 Brevik, Norway
petter.hemstad@heidelbergmaterials.com

Petter Kjellemyr, MSc.
Norner AS
Dokkvegen 20
3920 Porsgrunn, Norway
petter.kjellemyr@norner.no

Klaartje De Weerdt, Prof. Dr.
NTNU, Department of Structural Engineering
Richard Birkelandsvei 1a
7491 Trondheim, Norway
klaartje.d.weerdt@ntnu.no

ABSTRACT

Calcium-alumina-silicate-hydrate (C-A-S-H) is the main hydration product formed in Portland composite cement pastes. C-A-S-H is a key phase with regard to the strength and durability of concrete. Proper characterization of C-A-S-H is difficult due to intermixing with other phases, thus limiting the applicability of point scan analyses using scanning electron microscopy (SEM). Recent advances have enabled the use of hypermaps from energy dispersive spectroscopy (EDS) to investigate hydrate phases with better statistics. This study investigated how increased curing temperature and the inclusion of pozzolanic SCMs change the composition of the C-A-S-H, using the edxia plugin and SEM-EDS hypermaps. Composite cement pastes were cured at 20, 38, and 60°C for 180 days before analysis. We discuss the interpretation of the data from hypermaps in comparison to the traditional point scan approach.

Key words: SEM-EDS, characterization, C-S-H, SCM, fly ash, volcanic pozzolana.

1. INTRODUCTION

Concrete is one of the most used construction materials worldwide [1]. Hardened concrete is a composite material where aggregates are bound together with a cement paste that consists of different hydrates containing mainly Ca, Si, and Al oxides [2]. About 45-70 wt.% of the cement paste consist more specifically of calcium-aluminate-silicate-hydrate, referred to as C-A-S-H [3–6]. C-A-S-H is a key phase for many aspects of concrete, including porosity [7], durability [8–10], and strength development [11–13]. C-A-S-H consists of CaO layers alternated with chains of silicate tetrahedra in which alumina can take up bridging positions in the silicate chains [14–16]. The length of the silicate chains and the amount of bridging alumina tetrahedra are variable, resulting in a range of Ca/Si and Al/Ca ratios for C-A-S-H in different cement pastes [15].

When replacing part of the Portland cement with pozzolanic supplementary cementitious materials (SCMs), such as fly ash or calcined clay, the composition of C-A-S-H is affected [3, 4, 7, 17–21]. Pozzolans are richer in SiO_2 and Al_2O_3 and poorer in CaO compared to Portland cement (PC), and they thereby cause a decrease in the Ca/Si ratio and increase in Al/Ca ratio of the C-A-S-H. Curing temperature has also been shown to influence the composition of C-A-S-H [3, 4, 20]. Increasing the curing temperature can lead to an enhanced pozzolanic reaction of the SCMs providing more silicates and aluminates to the system and resulting in further decreased Ca/Si and increased Al/Ca ratios [20].

Due to the importance of C-A-S-H, much work has been done to improve methods to characterize its composition. Current state of the art methods are specialist techniques like transmission electron microscopy (TEM) or solid-state Si and Al nuclear magnetic resonance (NMR) [22]. However, scanning electron microscopy with energy dispersive X-ray spectroscopy (SEM-EDS) analysis of polished sections of hydrated cement paste has been widely used as a more accessible technique. One recognized approach for assessing the C-A-S-H composition using SEM-EDS involves manually selecting points of interest from a backscattered electron (BSE) map such as the map shown in Figure 1 a) [23].

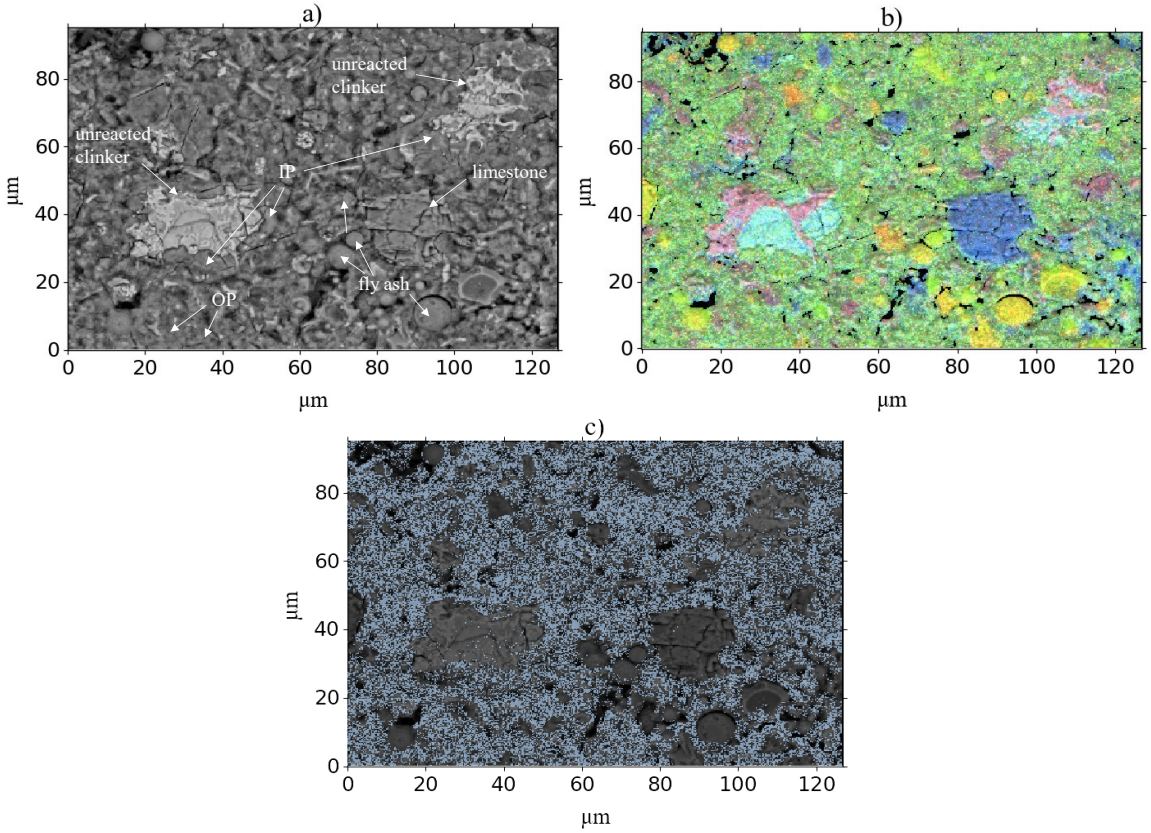

Figure 1: a) BSE image of the PC-FA specimen cured at 38°C used in the edxia. b) Composite 2D map with green (Si), blue (Ca) and red (Al). c) darkened BSE to highlight filtered data overlay using the elemental filter (blue = datapoints selected as IP+OP).

Determining the composition of C-A-S-H is difficult in part due to its nano-crystalline structure. The major limitation of SEM-EDS is the size of the interaction volume. The SEM electron beam using typical EDS settings (15 kV, 10 mm working distance, and high count-rate) generates X-ray signals from a volume of approximately 1 μm^3 [23]. This is much larger than the individual grains of C-A-S-H in the cement paste, which can be smaller than 10 nm [14]. This means that each point that is analysed contains a mixture of phases. To identify the phases within this volume, the results are plotted in 2D scatter plots of atomic ratios, typically Al/Ca vs Si/Ca. In the graph, the datapoint will be situated in between the ideal stochiometric atomic ratios of the phases it comprises. Figure 2 shows a 2D scatterplot with ideal stoichiometry indicators for ettringite (AFt, $C_6A\underline{S}_3H_{32}$), monosulphate AFm ($C_4A\underline{S}H_{11}$) and Portlandite (CH). As C-A-S-H has a variable composition, its atomic ratios are estimated using the edge of the cloud of points with the highest Si/Ca ratio. This region of the ratio plot corresponds to C-A-S-H with the lowest amount of other intermixed phases. While this approach is reported to agree with TEM results [23], it is susceptible to user bias when selecting points and graphically interpreting the atomic ratio plots.

Another approach for characterization is using elemental SEM-EDS maps rather than point scans. A method of merging different elemental maps to “hypermaps” was demonstrated by Münch et

al. [24]. The hypermaps contain complete EDS spectra for each individual pixel within the field of view analysed, which can be quantified to obtain the composition using the EDS software.

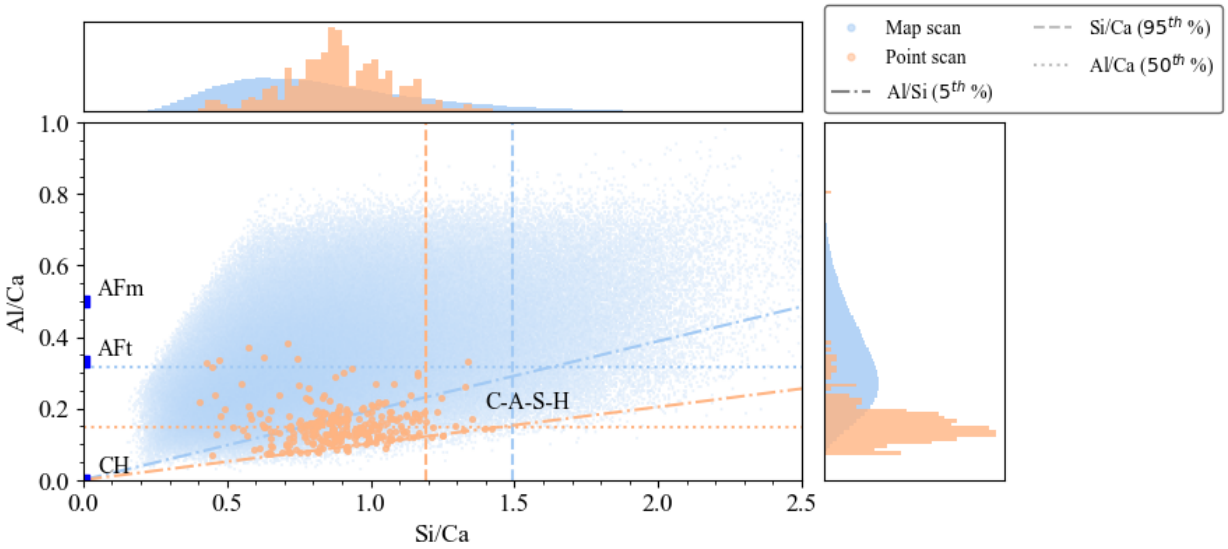

Figure 2: PC-VP cured at 20°C, with data from map scan (blue dots) and point scan (orange dots) method. Additionally, lines representing the 95th percentile of Si/Ca (vertical), 50th percentile of Al/Ca (horizontal) and 5th percentile of Al/Si (sloped) of each method in their respective colour. Markers for AFm (Al/Ca = 1/2), AFt (Al/Ca = 1/3) and CH (origo) are indicated on the y-axis. Histograms for Si/Ca (above) and Al/Ca (right side) show normalized distributions for both datasets.

Georget et al. [25] have developed a Python-based framework called edxia, which enables identification and quantification of phases in using SEM-EDS hypermaps. The edxia framework provides convenient access to several data processing algorithms useful for investigating the microstructure of cementitious materials. The default total-variation denoising algorithm [26] with the dependent weight variable set to 0.1 is applied to reduce the noise in each elemental map. Maps are typically collected with lower pixel dwell time than point scans, which makes the denoising a crucial step for improving the quality before further analysis. A composite map can then be generated by combining the elemental maps of Ca, Si and Al. These elemental maps are assigned to the corresponding colour channels of an RGB image (red = Si, green = Al, blue = Ca) and scaled using edxia's default parameters to highlight the colour range associated with the different phases (see Figure 1 b). To reduce the amount of data before further analysis, a superpixel segmentation algorithm is applied. This algorithm identifies adjacent pixels with similar composition and groups them into continuous regions, greatly reducing the number of datapoints without losing significant information. A filter based on the histograms derived from the scaled Si, Al and Ca elemental maps used in the composite map is applied to the grouped clusters to exclude unreacted phases such as C_4AF, C_2S, C_3S and SCM particles.

This study applies the edxia framework [25] to investigate the composition of C-A-S-H, focusing on the main elemental ratios Al/Ca, Al/Si and Ca/Si. This method offers several advantages compared to traditional point scan methods, including relatively fast processing, the potential for a more representative analysis due to the utilization of a larger dataset, and reduced user-bias. A

detailed step-by-step procedure to our data treatment approach with included Python scripts is provided as supplementary data to enable the reader to apply and further improve our approach.

Describing the C-A-S-H composition as a statistical distribution is different from the traditional graphical method, where single-value compositions are obtained. We compare results obtained with both methods and discuss their pros and cons. Should the C-A-S-H composition be described as a distribution rather than single values? If so, which statistical parameters should be used to describe it? Finally, steps to further improve the approach are proposed.

In this study we investigated a set of nine cured cement pastes made. We aimed to provoke changes in the C-A-S-H composition by including pozzolanic SCMs and varying the curing temperature. The pozzolanic reaction is expected to lower the Ca/Si and increase the Al/Si, and the curing temperature affects both the pozzolanic reaction and the composition of the hydrates. The reference cement paste contained 65% PC and 35% limestone (L). The composite cements with pozzolanic SCMs contained 25% fly ash (FA) or volcanic pozzolan (VP), and 10% L. The pastes were sealed cured at 20, 38 or 60°C, for a total of 180 days.

2. METHODS AND MATERIALS

2.1 Raw materials

The raw materials used in this project are Portland cement (PC), limestone (L), fly ash (FA) and volcanic pozzolan (VP). L was included as an inert reference to separate the effects of pozzolanic reaction from clinker dilution. They are all part of the NEWSCEM project (Norwegian Research Council project number 282578) with the characterization data provided in Table 1. Table 1 contains X-ray fluorescence (XRF) compositional analysis. Rietveld refinement for the PC and SCMs, as well as the particle size distribution are provided and discussed further in Hemstad et al. [3]. Table 2 gives the composition of the reactive parts of the raw materials as reported by Hemstad et al. [3]. All crystalline phases in the PC were all considered as reactive. In the other, all materials were considered non-reactive with the following exceptions: Calcite, belite, gypsum, periclase, lime, portlandite and anhydrite.

Table 1: Characterization of the Portland cement, limestone, fly ash and volcanic pozzolan. Included are element compositions determined by XRF given as oxides, median particle size (d_{50}) and Blaine specific surface area.

Material	**Portland cement [wt.%]**	**Limestone [wt.%]**	**Fly ash [wt.%]**	**Volcanic pozzolan [wt.%]**
SiO_2	19.6	13.2	55.1	47.4
Al_2O_3	4.7	3.3	21.6	13.7
TiO_2	0.3	0.2	0.9	1.5
MnO	0.1	0.2	0.1	0.2
Fe_2O_3	3.2	1.9	7.0	12.4
CaO	63.1	44.4	5.3	11.2
MgO	2.3	1.7	2.2	10.8
K_2O	1.1	0.8	2.1	0.3
Na_2O	0.4	0.2	0.9	1.7
SO_3	3.7	0.6	0.2	0.1
P_2O_5	0.1	0.0	0.7	0.2
LOI 950°C	1.3	-	-	-
LOI 1050°C	-	33.4	3.3	0.2
Sum	100.0	99.8	99.4	99.6
d_{50} [µm]	12.4	16.1	11.3	5.1
Blaine surface [m^2/kg]	453	402	450	733

Table 2: Composition of reactive parts of the raw materials normalized to 100 %.

Element	**PC**	**L**	**FA**	**VP**
	Amount of element in the reactive fraction of the materials [wt.%]			
CO_2	1.3	42.4	3.9	0.5
SiO_2	19.7	0.4	56.3	47.0
Al_2O_3	4.7	0.2	19.7	16.2
TiO_2	0.3	0.2	0.7	1.9
MnO	0.1	0.2	0.1	0.2
Fe_2O_3	3.2	0.2	5.8	12.2
CaO	63.4	53.8	6.3	13.1
MgO	1.1	1.2	1.6	7.0
K_2O	1.5	0.2	3.5	0.5
Na_2O	0.3	0.2	0.9	1.1
SO_3	4.3	0.9	0.2	0.1
P_2O_5	0.1	0.1	0.9	0.2
Sum	100	100	100	100

The reactive composition was calculated by subtracting the non-reactive composition calculated using QXRD from the total composition as determined with XRF (Table 1), see Hemstad et al. [3] for details.

2.3 Cement paste preparation

Table 3 gives an overview of the composition of the composite cements used along with the respective abbreviations. A cement with 35 wt.% L replacement was used as a reference, while the SCM replacements investigated were 25 wt.% FA and VP along with 10 wt.% L.

Table 3: Overview of the composite cements studied.

Full name	Abbreviation	PC [wt.%]	L [wt.%]	SCM [wt.%]
Portland cement with limestone	PC-L	65	35	0
Fly ash cement	PC-FA	65	10	25
Volcanic pozzolan cement	PC-VP	65	10	25

The pastes were mixed with a Braun MR5550CA high shear mixer, in batches of 375.0 g deionized water and 750.0 g cement (w/b ratio 0.50). The cement paste was first mixed at a medium speed for 1 minute, set to rest for 1 minute while agglomerated powder was scraped from the sides. After 1 additional minute of mixing the pastes were transferred to 20 mL polypropylene bottles sealed with lids and parafilm. They were set to cure submerged in deionized water in temperature-controlled environment at 20, 38 and 60°C for 180 days. The cement paste samples were then cut into slices using a precision saw (IsoMet1000) with water cooling. To avoid bleeding and sedimentation, a 3 mm section from the middle of the sample was used for SEM-EDS investigation. Hydration was subsequently stopped by immersion in 30 mL isopropanol for at least 3 days, before being decanted off and further dried in a vacuum desiccator at -0.2 bar overnight.

Polished sections were produced at DTI in Denmark. The hydrated cement pastes were impregnated with an epoxy resin (Epoxy technology, EPO-TEK 302 8OZ) under vacuum (-25 bar, Buehler Cast N' Vac 1000). Polished sections were achieved by manual polishing, using a Metkon FORCIPOL 300-1 V equipped with a Metkon FORCIMAT specimen mover.

A layer of carbon coating was utilized to ensure a conductive surface before the sample was mounted on a brass stub using carbon and copper tape. The instrument used for this study was a Hitachi S-3400N with a tungsten filament (SEM) and a 80 mm^2 X-MAX silicon-drift detector (EDS) by Oxford instruments. Results from EDS were processed using the Aztec software.

2.3 SEM-EDS

Point analysis, Graphical method

The traditional way of conducting SEM-EDS for compositional analysis in cement pastes involves manually selecting points of interest following the procedure described by Scrivener et al. [23]. By locating partially unreacted grains, it is possible to manually select points of inner product (IP) within the original clinker grain and outer product (OP) out in the paste matrix. The recommended number of sites for cement paste are around 20 images given a field of width of a few hundred microns [23]. Additionally, it was suggested to acquire no more than 20 points per site. For this study, the point analyses were acquired with an accelerating voltage of 15 kV and a probe current optimised for incoming counts and a dead time of about 20-30%. The working distance was set to approximately 10 mm, and 250,000 counts were acquired for each pixel. For each cement paste, 4-5 sites with approx. 60-70 point analyses each were collected, resulting in ca. 300 point analyses per cement paste. A map scan was acquired from each site prior to point analysis, with a dwell

time of 100 µs/pixel. The investigated sites had a size of 127 µm x 95 µm (magnification x1000), and a number of pixels 1024 x 768, resulting in a pixel size of 0.124 µm.

The EDS datapoints were plotted in atomic ratio plots with Si/Ca in the x-axis and Al/Ca on the y-axis. Since each point is a mixture of phases, the composition of the point will be located between the pure compositions of those phases. Figure 2 illustrates this approach. For points acquired from IP, C-A-S-H will be the phase with the highest Si/Ca and lowest Al/Si ratios. Any intermixing with CH or AFm/AFt will reduce the Si/Ca ratio, whilst intermixing with AFm/AFt also increases the Al/Si ratio. It is therefore assumed that the composition of pure C-A-S-H can be found as the lower rightmost corner of the scattered point cloud, as shown in Figure 2.

To minimize reliance on subjective interpretation of the Al/Ca vs Si/Ca plot to determine the C-A-S-H composition, a general criterion was established by Hemstad et al. [3, 4]. They determined that for Si/Ca the 95th percentile of Si/Ca (equivalent to the 5th percentile of Ca/Si) could be used. For Al/Ca, the manual selection based off the point cloud corresponded well with the 50th percentile of Al/Ca, which corresponded to the 5th percentile of Al/Si.

Map analysis, statistical method
Sites for map scans were selected by locating unreacted clinker grains of appropriate size to acquire a significant number of data points from the inner product (IP). Instead of individually selecting points, each pixel in the map scan was treated equivalently to a point scan. The pixel values for all elements were exported from the Oxfords EDS software, Aztec.

After acquiring the EDS map scans they were computed into quantmaps. This process takes the hypermaps containing the complete EDS spectra for each pixel and quantifies them to obtain the elemental composition in each pixel. Compared to manually selecting points, the map scan approach greatly reduces the time spent on data acquisition but adds approximately 15 minutes of minimal post processing for the quantification per site.

2.4 Data processing

Glueviz with the edxia plugin [25] was used to filter and plot the map scan data. Glueviz is a Python library used to explore the relation between the datasets. It was used to construct a layered dataset from the individual elemental hypermaps obtained from the Aztec software and connect them as positional pixel data. The edxia framework then provided further processing algorithms useful for investigation of the microstructure of cementitious materials.

Since the equipment used was a standard grade EDS and the map scans were acquired with relatively short pixel dwell time, the resulting maps were typically noisy. A denoising algorithm was therefore used to remove artifacts. This is an important step to improve the quality of the image before further analysis. Optimally, the denoising algorithm should reduce high frequency spots, while maintaining sharp edges between phases. The total-variation algorithm [26] was used for denoising based on the recommendation from Georget et al. [25]. Only one dependent weight variable was used, which was set to the default value of 0.1.

Further data processing involved creating a composite map by combining elemental maps. To separate the phases present in a cementitious system, the main elements to focus on are Si, Al and Ca. These elemental maps are subsequently scaled according to default values, to adjust the range of colours, and assigned to corresponding channels of a RGB image (red = Si, green = Al, blue = Ca) which are used to form the composite map (Figure 1 b). A superpixel segmentation algorithm was applied to reduce the number of datapoints (from 1024x768 to ≤ 20,000). This algorithm identifies adjacent pixels of similar composition and groups them into continuous regions.

Lastly, edxia was used to develop a filter to exclude clusters of unreacted minerals as further described further in section 3.1. By establishing this filter using the cluster data rather than the pixel data, the unwanted phases were easier to exclude since some filtering was already done by the segmentation algorithm. This also reduced the computation time as fewer points had to be treated. For further assessment of the data, the filtered points were correlated back to the original pixels. The filtering reduced the size of the dataset by 65-70%.

The map scan method is limited by the size of the electron beam interaction volume, even if the filter removes unreacted phases and phase boundaries from the data. The map scan data contains pixels (0.124 μm) that are smaller than the interaction volume (1 μm^3). Each pixel therefore contains information on the phases present in neighbouring pixels. To address this issue, the data from each pixel within a given site was considered as dependent on the other nearby pixels.

3. RESULTS AND DISCUSSION

3.1 Filtering

Since this study was concerned with the composition of C-A-S-H, the data had to be filtered in a way that removed other phases. Ideally, pixels from the hypermaps that contained pure C-A-S-H (unmixed IP) or a mixture of mostly C-A-S-H and other phases (OP) would be the only ones that get past the filter. This process has many challenges [27], but a filter based on the atomic% of Si, Al, and Ca was used with reasonable success. We applied the following limits to the dataset: Si between 0.30 and 0.76 atomic%, Al between 0.16 and 0.35 atomic%, and Ca between 0.27 and 0.54 atomic%, with the purpose of filtering out the data related to unreacted clinker, limestone and SCMs. One way of verifying whether the filter was successful in excluding this data is by visually inspecting BSE images. Figure 1 demonstrates how the filter selects the hydration phases, further referred to as the matrix, in the PC-FA paste cured at 38°C. Figure 1 a) shows the BSE image and Figure 2 b) the corresponding composite map with green (Si), blue (Ca) and red (Al). The unreacted clinker (bright unreacted C_4AF phase rich in Al, and in between bright unreacted C_2S or C_3S), limestone (homogenous grey and rich in Ca) and some fly ash particles (spherical rich in Si) are indicated in the BSE image. The points selected after applying the elemental filter are shown overlayed on the BSE image in Figure 1 c). The unreacted clinker, FA, and limestone are clearly excluded from the filtered data. Even though some filtered pixels can be spotted in the unreacted clinker grains, their presence are negligible when compared to the overwhelming number of pixels representing the matrix phase. Thus, the filter was successful in excluding the unreacted material, and after applying the filter about 30-35% of the data collected were selected.

These points were comprised of C-A-S-H (IP and OP) intermixed with other minor phases present in the matrix.

Figure 3 a) shows Al/Ca vs Si/Ca scatter plots for all data collected (dark grey) and the data filtered using the elemental filter (blue). In addition, histograms for the Si/Ca (above) and Al/Ca ratio (right side) are added to illustrate the frequency of the ratios in the datasets. Note that the area underneath the histograms is not normalized to illustrate the reduction in data when applying the filter. Figure 3 a) and b) show the same data, where a) shows a wider range of ratios and b) zooms into the area relevant for C-A-S-H. Figure 3 a) appears to show a lot of datapoints with relatively high Si/Ca ratios (>2) and Al/Ca ratios (>1). However, the histograms show that these points only represent a small fraction of the entire dataset, at most 13-15%. Most points are located at lower Al/Ca and Si/Ca ratios. The density plot in Figure 3 b) gives a more realistic view of all the overlaying points, where a higher colour intensity represents more points.

A red dashed line with an Al/Si slope of 0.461 starting from the centre of the C-A-S-H point cloud is included in Figure 3 a). The slope of this line represents the Al/Si ratio of the FA. The idea was to check whether datapoints would gather along this characteristic slope associated with FA. These datapoints would then relate to datapoints collected in unreacted FA particles. This would allow us to potentially create a filter to remove the unreacted FA particles. However, there was no clear trend of points concentrating along the red dashed line. The FA particles likely vary in composition as they are heterogenous and contain various glass phases and minerals, which could explain why we do not see a concentration of points stretching along or parallel to the red dashed line [28].

The dashed lines representing the 95^{th} percentile of Si/Ca, the 50^{th} percentile of Al/Ca and the 5^{th} percentile of Al/Si of the filtered dataset are marked in Figure 3 b). As discussed in section 2.3.1 these parameters can be used to locate the edge of the point cloud associated with C-A-S-H and to estimate the C-A-S-H composition (see also Figure 1). The three curves for Si/Ca, Al/Ca, and Al/Si intersect nearly in one point. This point can be used to find a unique composition of C-A-S-H analogous to the point scan method.

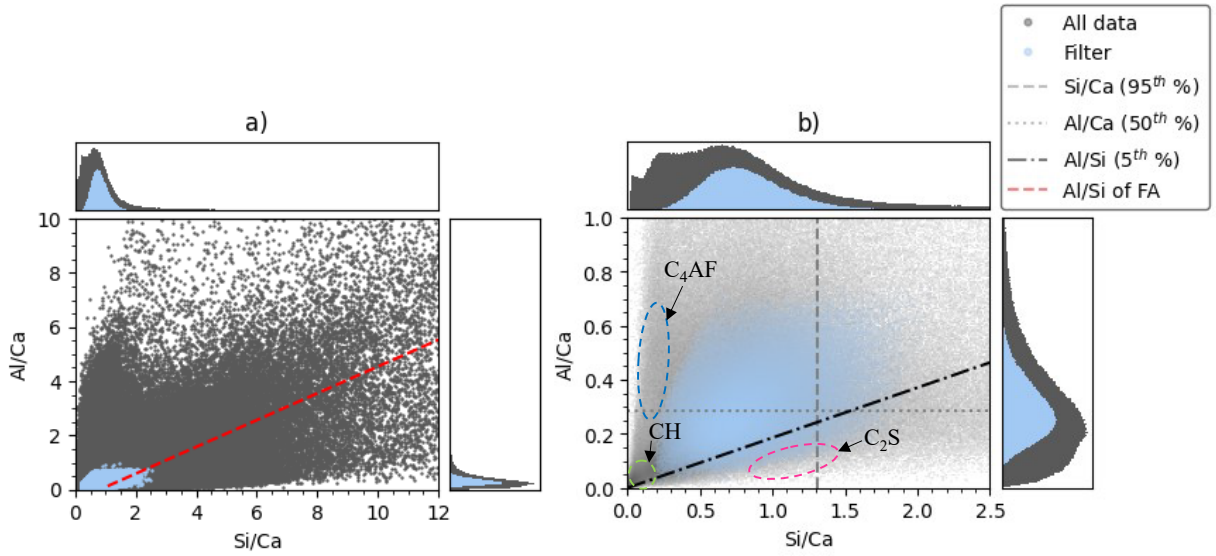

Figure 3: a) Al/Ca vs. Si/Ca scatter plot with histograms for PC-FA, cured at 38°C, showing both all data (grey) and data filtered with elemental filter 1 (blue), zoomed out to cover high ratios and including a red dashed line indicating the Al/Si ratio of FA; b) Al/Ca vs. Si/Ca density plot (more points gives higher intensity) with histograms, the intersecting precentile lines of the filtered data are used to estimate the C-A-S-H composition. Histograms are not normalized to show the reduction in data caused by filtering.

3.2 How many sites should be analysed to ensure representativeness?

As discussed in Section 2.3, the point scan method recommends selecting 20 sites, with no more than 20 points per site, resulting in 400 datapoints to obtain a representative dataset. When collecting full map data, approximately 800,000 pixels/datapoints are acquired for an image of 127 by 95 µm. Even after filtering out the unreacted phases, approximately 300,000 datapoints remain. With this increased amount of datapoints compared to the point scan method, it may be possible to reduce the required number of sites without compromising the representativeness of the dataset.

The paste with PC-FA cured at 60°C was used as an example to determine the necessary number of sites for statistical significance. The fitting of Si/Ca ratios were best described by a gamma distribution with a shape factor α of approximately 4. A selection of the fitted distributions and further parameter details for the gamma distribution can found in the Supplementary Data.

Considering first the Si/Ca values, each site has a large standard deviation. The deviation is approximately 40% of the mean value of Si/Ca (see Table 5 in Appendix A). However, this property appears consistent between sites and for different cement pastes. All sites from the same sample show a similar mean value, suggesting that the method effectively captures the complete distribution in each map scan. The independence of the data between sites was maintained by ensuring sufficient spacing between them.

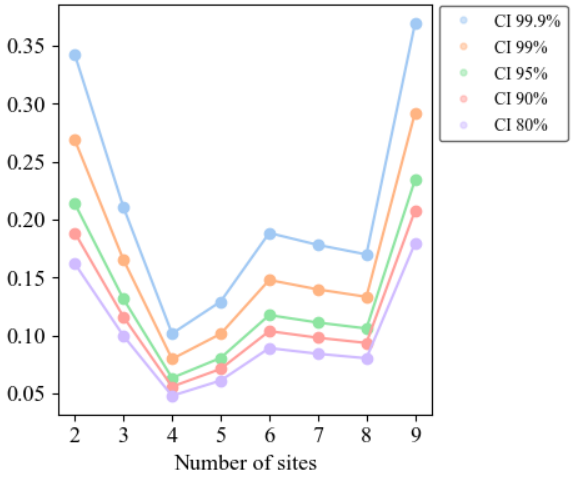

Figure 4: Confidence interval of PC-FA cured at 60°C, around an average Si/Ca-ratio of 0.8 at.%. The confidence interval was calculated for confidence levels of 80 to 99.9% allocated different colours.

Figure 4 displays the confidence intervals (CI) for the mean Si/Ca of 0.8 atomic% as a function of number of sites, calculated based on a gamma distribution with confidence levels ranging from 80-99.9%. To account for the pixel dependency, the mean and standard deviation were calculated individually for each site. Subsequently, the confidence interval was determined using the overall mean and standard deviation corresponding to the number of sites. The length of the CI represents the total difference between the lower and the upper boundary around the mean value. Increasing the number of sites shows that the confidence interval remains reasonably stable for 9 sites, indicating that no major discrepancies are found in the investigated range. Similar patterns where also observed for the Al/Ca ratio, although it was slightly better described by a beta distribution. Based on this observation, 3 sites per cement paste sample were chosen as a reasonable compromise between time for analysis and confidence in the result. From this point on, map data results are based on data combined from 3 sites per sample.

3.3 Comparative analysis of the point scan and map scan method

The following sections will cover the observations regarding the C-A-S-H composition when incorporating pozzolanic SCMs compared to the reference limestone cement, as well as the effect of varying curing temperature.

The graphs used in Figure 5 and Figure 7 are density plots which are an adaptation of the traditional scatter plots. The colour intensity of the dots is based on the number of points within the binned area, such that more intense colours represent a larger number of points. The density plots effectively address the issue of overlapping points that could be deceiving in scatter plots, giving a more intuitive understanding of the point distribution. Given the extensive amount of data evaluated, histograms for each axis are included (Si/Ca on top and Al/Ca on the right-hand side). Figure 5 and Figure 7 both convey the same information; however, Figure 5 enables the comparison of all composite cements at a particular curing temperature, and Figure 7 all curing temperatures for a specific composite cement.

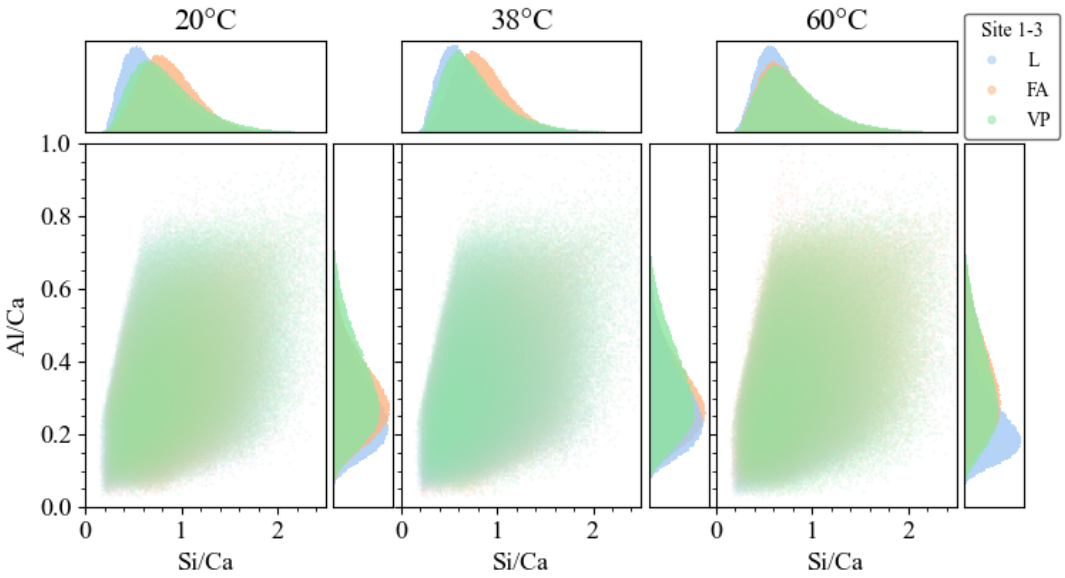

Figure 5: Density plot of Al/Ca vs. Si/Ca ratios for PC-L, PC-FA and PC-VP at 20, 38 and 60°C, with each SCM displayed as a function of temperature.

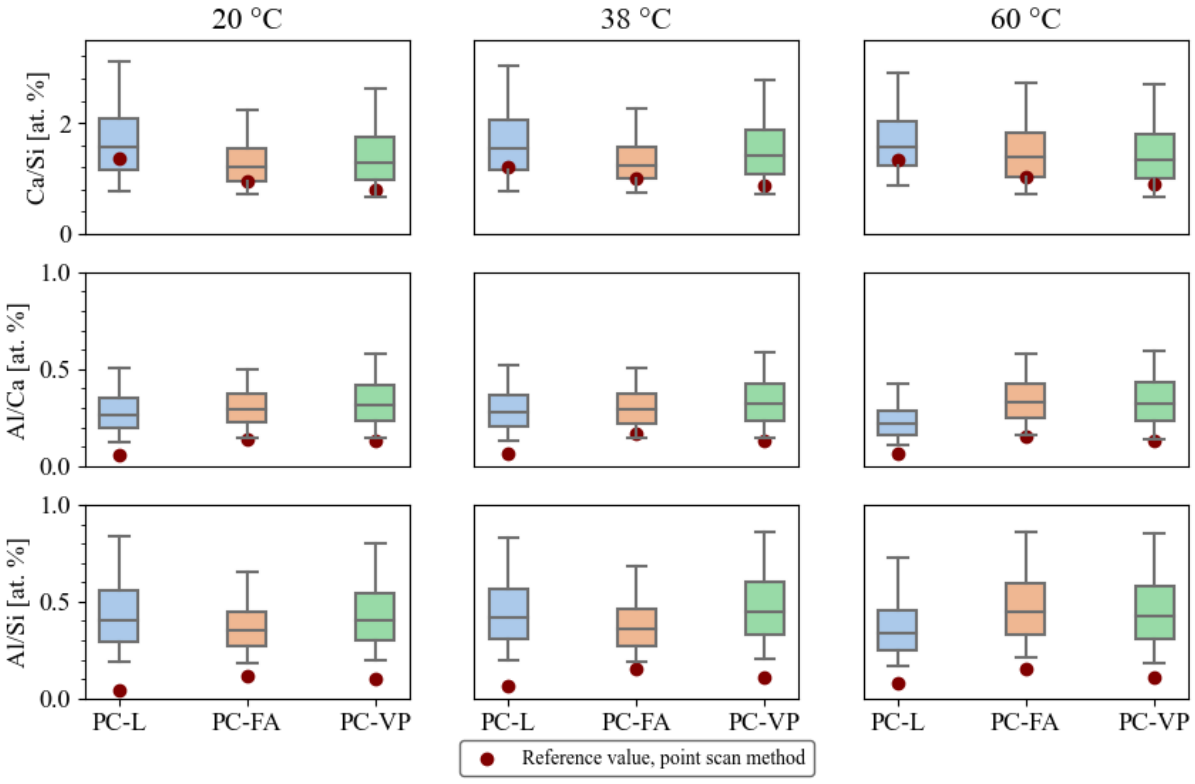

Figure 6: Boxplot of Ca/Si, Al/Ca and Al/Si ratios for PC-L, PC-FA and PC-VP at 20, 38 and 60°C, where Ca/Si and Al/Ca reference points (red dots) are given at 5th and 50th percentile respectively.

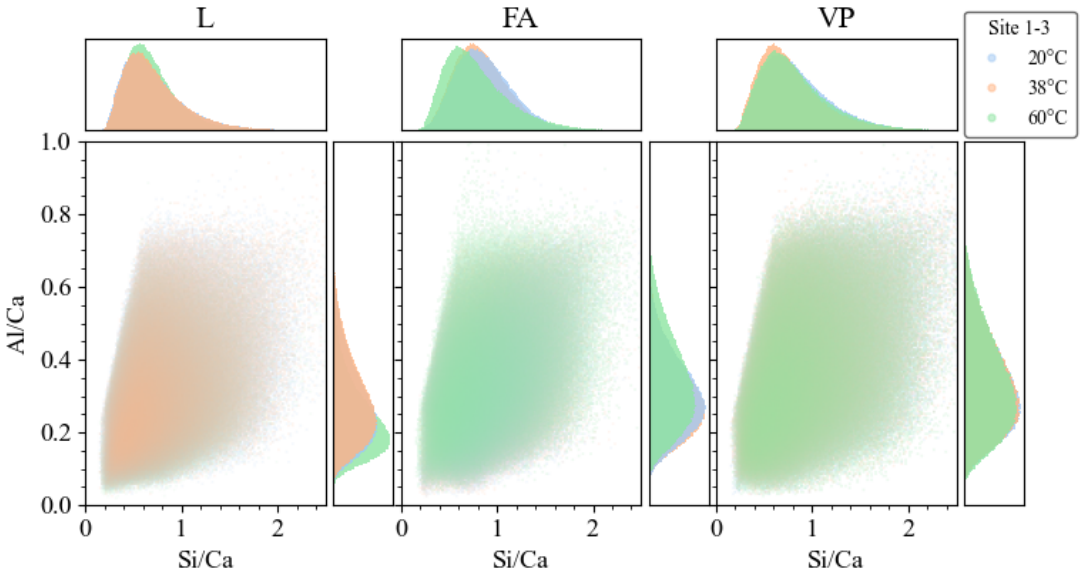

Figure 7: Density plot of Al/Ca vs. Si/Ca ratios for PC-L, PC-FA and PC-VP at 20, 38 and 60°C, with each temperature is displayed as a function of SCM. The PC-L window (left) shows the specimen cured at 38°C (orange) in front to avoid overlapping.

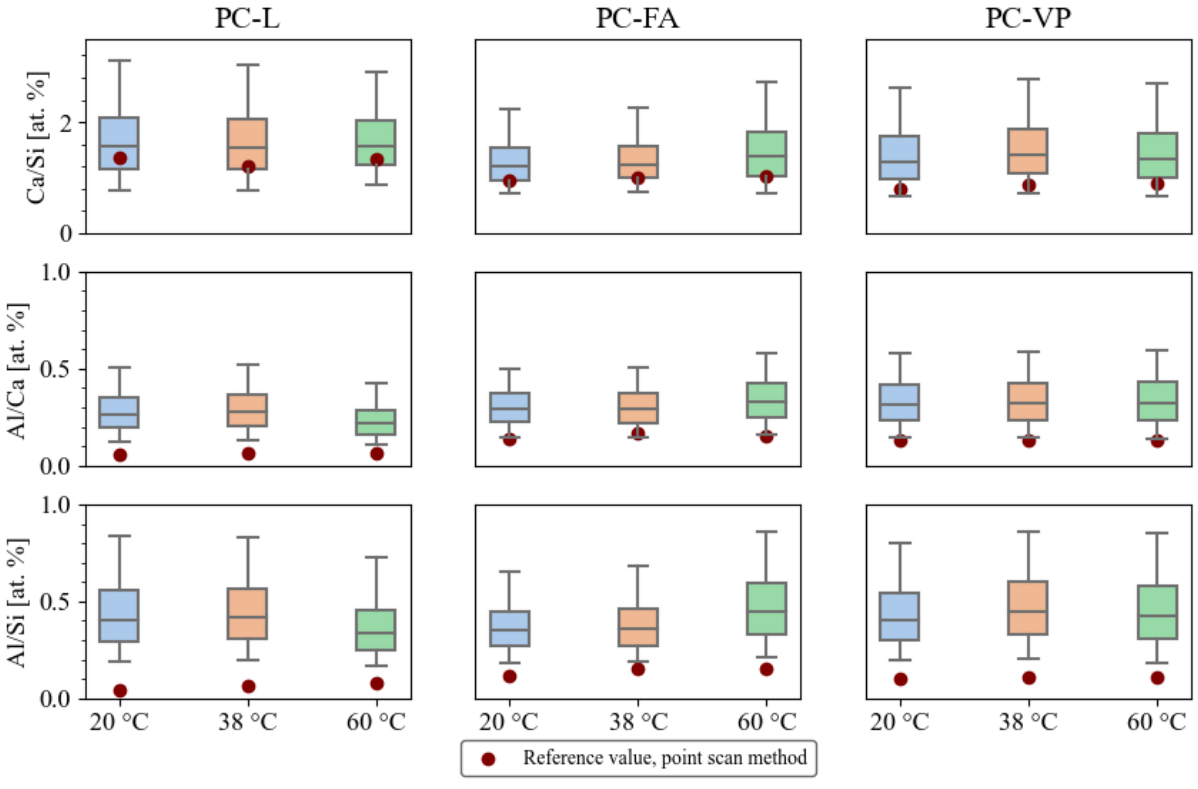

Figure 8: Boxplot of Ca/Si, Al/Ca and Al/Si ratios at 20, 38, and 60°C for PC-L, PC-FA and PC-VP from map scan data, and Ca/Si and Al/Ca reference points (red dots) obtained with the point scan method being the 95th and 50th percentile respectively.

In addition to the density plots, Figure 6 and Figure 8 depict box plots, similarly grouped as before, providing valuable insight into the distribution of the data. The boxplots are presented with whiskers at the 5th and 95th percentile, the box edges indicating the 25th and 75th percentile and a line inside the box at the 50th percentile (median). All potential outliers, i.e., datapoints outside of the 5th and 95th percentile are taken into account. They are however not displayed as they account for a negligible portion of the dataset, and are likely to be affected by intermixing with other phases. Also included in the boxplots are red markers indicating the atomic ratios determined by Hemstad et al. [4] using the point scan method for the same cement paste.

The point scan method is normally used to find single values for the atomic ratios of C-A-S-H. However, since multiple points are acquired, it is possible to describe the distribution of the points in the same ways as for map scans. As Figure 2 shows, the distributions of Al/Ca and Si/Ca are very different for the two methods, but they can still be compared. Table 4 gives the percentiles from the atomic ratio distributions of the two different methods that gave similar values for Ca/Si and Al/Ca. These percentiles are therefore used in the following discussion. Additional percentiles including the median are provided in Appendix A.

Table 4: The percentiles which give comparable values for the composition of C-A-S-H determined by point scan and map scan methods.

Property	Point scan [percentile]	Map Scan [percentile]
Ca/Si	5th	25th
Al/Ca	50th	5th

The 5th percentile of Ca/Si of the PC-L reference cured at 20 and 60°C determined by point scan is consistently 0.1 to 0.2 at.% larger than that of the 25th percentile from the map scan data. For the PC-L reference cured at 38°C however, there is a good correlation between the 5th percentile from point scan with the 25th percentile of the map scan. Similarly, the Ca/Si ratio of PC-FA determined by point scans correlates well with the 25th percentile of the map data for all curing temperatures. The point scan values for PC-VP have their 5th percentile between the 5th and 25th percentile of the map scan data, approximately 0.1 to 0.2 at.% below the 25th percentile.

When considering the Al/Ca ratio, the 50th percentile from point scan data correlates quite well with the 5th percentile of map scan data. The largest discrepancy is seen for the PC-L reference where the 50th percentile of the point scans are approximately 0.06 at.% smaller than the 5th percentile of the map scan. It is however important to note that it is difficult to observe trends in the 5th percentile of map scan data, which could be explained by instrumental limitations, where lower concentrations are more challenging to detect.

Considering the comparatively small number of datapoints collected with the point scan method, it is possible that the user bias in the point selection process consistently favours areas with higher Ca/Si or lower Al/Ca content. The map scans are likely overestimating the Al/Ca ratio due to intermixing of Al from AFm and AFt. It is also possible that the filtering process results in incorporation of additional phases not related to C-A-S-H. It is therefore crucial to evaluate the methodology and potential biases to ensure the reliability and accuracy of the results presented.

3.4 Variations in C-A-S-H composition

Figure 5 shows the filtered data collected from the different cement blends, PC-L (blue), PC-FA (orange) and PC-VP (green), for each curing temperature. By comparing the different SCMs at each curing temperature, it is easier to show how the individual SCMs affect the C-A-S-H composition. Considering the amount of SiO_2, Al_2O_3 and CaO available in the reactive composition of the raw materials L, FA and VP (Table 2) we would expect that the Ca/Si ratio to decrease when replacing PC with pozzolanic SCMs like PC-FA < PC-VP < PC-L, and Al/Ca to increase from PC-L < PC-VP < PC-FA as observed for similar systems in [17, 20, 21]. The complementary box plots in Figure 6 assist in the interpretation of the density plots and histograms. Table 5, Table 6 and Table 7 in Appendix A report the numerical values in at.% for Ca/Si and Al/Ca and Al/Si represented in the box plots.

The expectation that the inclusion of SCMs would result in a decrease in Ca/Si ratio compared to the limestone reference was confirmed by the data. For all investigated temperatures, the 25th percentile of the Ca/Si determined with the map scan method (Table 5, or lower edge of the box in Figure 6) for cement pastes containing FA and VP ranges from 0.95 to 1.03 at.%, while L is slightly higher at 1.15 to 1.22 at.%. The Ca/Si ratios determined with the point scans (5th % in Table 5 or red dots in Figure 6) tend to be slightly higher than the ones determined with the map scans for the PC-L pastes, i.e., 1.19 to 1.35 at.%, and slightly lower for the PC-VP pastes, i.e., 0.79 to 0.89 at.%, thereby indicating an even stronger lowering effect of the VP on the Ca/Si ratio. Note that both the Ca/Si ratios determined by the map and point scans are rather low compared to values reported in literature [17, 20] which are more in the range of 1.1-1.8 for similar replacement levels and curing ages and temperature, which is more in the range of the median values reported in Table 5.

The Al/Ca ratio is expected to increase upon including aluminate rich pozzolanic SCMs. This is, however, not clearly supported by the data as the 5th percentile values from the maps scans for PC-L, PC-VP and PC-FA (Table 6 and Figure 6) are all fairly similar, and in the range of 0.11 to 0.16 for all investigated temperatures. The limestone pastes are at the lower end, whilst FA and VP are at the higher end, but the differences are rather small. This is also apparent in the overall distribution. The Al/Ca ratio obtained with the point scan method (50th % in Table 6 and red dots in Figure 6) is considerably lower than that obtained by the map scan method for the PC-L paste, i.e. 0.06-0.07, but similar for the PC-FA and PC-VP pastes, meaning that point scan method indicates a clearer contribution of the SCMs to the aluminate uptake in the C-A-S-H. The overall Al/Ca ratios obtained in this study are in the same range as the ones reported in literature for similar systems, i.e. 0.13-0.17 [20].

The curing temperature did not appear to influence the amount of data that was filtered. Using PC-VP as an example, around 25% of the map points pass the C-A-S-H filter regardless of temperature. For PC-FA the number is 35%, but the temperature behaviour is the same.

Similarly to Figure 5, Figure 7 shows the filtered data collected from cement pastes cured at 20 (blue), 38 (orange), and 60°C (green) for each composite cement. The complimentary boxplots in Figure 8 are used to investigate the temperature effect on the Ca/Si, Al/Ca and Al/Si ratios.

The 25th percentile of the Ca/Si ratio from the map scan method for PC-L remains unaffected by a temperature increase from 20 to 38°C, suggesting that the overall composition remains constant within this temperature range. However, at 60°C, the distribution of the Ca/Si ratio increases slightly from 1.15 to 1.22 while maintaining a constant median value. This could potentially suggest that curing at an elevated temperature leads to a more homogeneous system. However, no clear increase in the 5th percentile Ca/Si ratio determined by point scan method was observed.

In the case of PC-FA, there is a small, but consistent increase in the 25th percentile of the Ca/Si ratio determined by the map scan method with higher curing temperatures. It is valid for the entire distribution (Figure 8, Table 5). This agrees with the point scan method (5th % in Table 5). These observations go against the expected result of higher temperature leading to a higher degree of reaction for FA, thereby making more Si available to the C-A-S-H and lowering its Ca/Si ratio.

Regarding the pastes with VP, there is no clear curing temperature dependency of the Ca/Si ratio determined by the map scan method. The point scan method (5th % in Table 5) on the other hand shows a slight increasing trend with increasing curing temperature, similar as for the FA pastes.

For the PC-L specimen, the Al/Ca ratio at 20 and 38°C determined by the map scan method are similar, but a slight decrease is observed at 60°C. The point scan results did not confirm this and indicated that the Ca/Al ratio was rather independent of the curing temperature.

As for PC-FA and PC-VP, no significant changes in the Al/Ca are observed with increasing the curing temperature using the map scan method, except for a slight increase for the PC-FA paste at 60°C. The point scan data did not show any clear curing temperature dependency of the Al/Ca ratio either for the PC-FA and PC-VP paste.

3.5 Further work

The approach presented here has room for improvements in several aspects, particularly in the preparation of the paste samples, the instrument settings, and the data filtering process. Preparing polished paste sections involves steps that can disturb the paste chemistry, such as leaching from cutting with a water-cooled saw, or from stopping hydration by submersion in 2-propanol.
This study was intentionally performed using a SEM-EDS that is representative of commonly available equipment in commercial and university laboratories. It has limited resolution and a wider electron beam compared to more state-of-the-art equipment like an electron probe micro analyser (EPMA), nuclear magnetic resonance (NMR) or TEM. The EDS was also not directly calibrated with a standard, but rather by an internal ZAF correction. Future studies could consider calibrating with reference samples that have similar Ca, Si, and Al content as cement pastes.

Edxia features several tools for optimizing the data treatment of hypermaps. While this study has investigated the possibility of using EDS map scan method, a better understanding of the statistical algorithms, mainly the denoising and segmentation algorithms, is needed to fully optimize the filtering of phases. In addition to this, the elemental filter developed for this study was limited to

three elements (Si, Al, and Ca). This could also be expanded to include Fe, Mg, S, or other elements that could help filter unwanted phases and avoid excluding C-A-S-H.

Choosing an optimal method for determining the composition of C-A-S-H remains a topic of discussion and warrants further investigation [27]. It is possible that describing C-A-S-H as a single phase with fixed atomic ratios throughout the entire cement paste might not adequately capture the inherent variability of this complex hydrate. After optimizing the method, it would be interesting to apply it for further studies of C-A-S-H and its properties. An example is the adsorption of various ions like alkali metals or sulphate onto the C-A-S-H surface.

4. CONCLUSIONS

This study uses the EDS hypermap approach and the edxia framework to investigate the composition of C-A-S-H in hydrated cement pastes. The results were compared to results on the same samples from more conventional point scan analyses. Three different Portland composite cement pastes were cured for 180 days at 20, 38, and 60°C. The reference limestone (L) cement contained 65% PC and 35% L. The Portland composite cements consisted of 65% PC combined with 25% of the pozzolanic SCMs fly ash (FA) and volcanic pozzolan (VP) with 10% L. All pastes had w/b ratios 0.50.
Elemental maps were captured using a SEM-EDS. These maps were layered and combined in hypermaps. A filter was developed which was able to remove the data associated with the unreacted clinker and SCM from the dataset. The remaining data were mostly from regions rich in C-A-S-H and accounted for approximately 30% of the overall data collected. Data from three sites were sufficient to estimate the C-A-S-H composition.

When comparing the C-A-S-H composition determined using manual point scan scatter plots (point scan method) with the distribution of atomic ratios of filtered area scan (map scan method), the 5^{th} percentile of the Ca/Si ratio for the point scan method correlated relatively well with the 25^{th} percentile from the map scan method, besides a slight underestimation in the case of PC-L and overestimation for PC-VP. Similarly, the 50^{th} percentile of the Al/Ca ratio from point scans correlates with the 5^{th} percentile from the map scan method, except for the PC-L paste which yielded considerably lower values with the point scans.

The addition of pozzolanic SCMs such as FA and VP consistently resulted in a lower Ca/Si ratio compared to the PC-L reference independent of the curing temperature or method used. When looking at the 5^{th} percentile of Al/Ca from the map scan method, all specimens seemed similar with approx. 0.14 at.% at 20°C. The point scan method on the other hand showed a clear increase in the Al/Ca from 0.06 at.% for PC-L to approx. 0.14 at.% for PC-FA and PC-VP, indicating that the pozzolans lead to an increase in the Al uptake in the C-A-S-H at 20°C, as expected.

Curing temperature variations did not show any major impact for Ca/Si ratio of the PC-L reference, however slight increasing trends were observed for PC-FA and PC-VP with both methods. The Al/Ca ratios for all composite cements are unaffected by variations in curing temperature, independent of the method used.

ACKNOWLEDGEMENTS

This paper is based on the MSc. thesis of Petter Kjellemyr which was a collaboration between the Faculty of Natural Sciences and the Faculty of Engineering at NTNU. We would like to acknowledge the Adj. Prof. Harald Justnes assisting as supervisor, Dr. Tobias Danner as external sensor and Prof. Ida Westermann as internal sensor, for facilitating this collaboration. We extend our thanks to Dr. Pamela Zuschlag for her prior work on the NEWSCEM project, as well as the partners in the project for supplying the materials. Lastly, we would like to thank Heidelberg Materials Global R&D for providing characterization of the raw materials, and Mikael Dissing at DTI for preparing polished sections.

REFERENCES

1. Scrivener, K. L., John, V. M., and Gartner, E. M., “Eco-efficient cements: Potential economically viable solutions for a low-CO2 cement-based materials industry”. *Cement and Concrete Research*, V. 114, 2018, pp. 2–26.
2. Taylor, H. F. W., “Cement Chemistry”. Thomas Telford, 1997.
3. Hemstad, P., Zuschlag, P., Kjellemyr, P., Lindgård, J., Kjellsen, K. O., Rønning, T. F., Justnes, H., and De Weerdt, K., “Alkali Metal Distribution in Composite Cement Pastes and its Relation to Accelerated ASR Tests”. *Cement and Concrete Research*, V. 173, 2023, p. 107283.
4. Hemstad, P., Lothenbach, B., Kjellsen, K. O., and De Weerdt, K., “The effect of varying cement replacement level on alkali metal distribution in cement pastes”. *Cement and Concrete Composites*, V. 146, 2024, p. 105344.
5. Durdziński, P. T., Ben Haha, M., Zajac, M., and Scrivener, K. L., “Phase assemblage of composite cements”. *Cement and Concrete Research*, V. 99, 2017, pp. 172–182.
6. Adu-Amankwah, S., Black, L., Skocek, J., Ben Haha, M., and Zajac, M., “Effect of sulfate additions on hydration and performance of ternary slag-limestone composite cements”. *Construction and Building Materials*, V. 164, No. 11, 2018, pp. 451–462.
7. Lothenbach, B., Scrivener, K. L., and Hooton, D., “Supplementary cementitious materials”. *Cement and Concrete Research*, V. 41, No. 12, 2011, pp. 1244–1256.
8. Machner, A., Bjørndal, M., Šajna, A., Mikanovic, N., and De Weerdt, K., “Impact of leaching on chloride ingress profiles in concrete”. *Mater Struct*, V. 55, No. 1, 2022.
9. De Weerdt, K., Wilson, W., Machner, A., and Georget, F., “Chloride profiles – What do they tell us and how should they be used?”. *Cement and Concrete Research*, V. 173, 2023, p. 107287.
10. Hong, S.-Y., and Glasser, F. P., “Alkali sorption by C-S-H and C-A-S-H gels”. *Cement and Concrete Research*, V. 32, No. 7, 2002, pp. 1101–1111.
11. Zunino, F., and Scrivener, K. L., “The influence of the filler effect on the sulfate requirement of blended cements”. *Cement and Concrete Research*, V. 126, 2019, p. 105918.
12. Bérodier, E. M., Muller, A. C. A., and Scrivener, K. L., “Effect of sulfate on C-S-H at early age”. *Cement and Concrete Research*, V. 138, 2020, p. 106248.
13. Valentini, L., Dalconi, M. C., Favero, M., Artioli, G., and Ferrari, G., “In-Situ XRD Measurement and Quantitative Analysis of Hydrating Cement: Implications for Sulfate Incorporation in C-S-H”. *J. Am. Ceram. Soc.*, V. 98, No. 4, 2015, pp. 1259–1264.

14. Richardson, I. G., “Tobermorite/jennite- and tobermorite/calcium hydroxide-based models for the structure of C-S-H: applicability to hardened pastes of tricalcium silicate, β-dicalcium silicate, Portland cement, and blends of Portland cement with blast-furnace slag, metakaolin, or silica fume”. *Cement and Concrete Research*, V. 34, No. 9, 2004, pp. 1733–1777.
15. Richardson, I. G., “Model structures for C-(A)-S-H(I)”. *Acta crystallographica Section B, Structural science, crystal engineering and materials*, V. 70, Pt 6, 2014, pp. 903–923.
16. L’Hôpital, E., Lothenbach, B., Le Saout, G., Kulik, D. A., and Scrivener, K. L., “Incorporation of aluminium in calcium-silicate-hydrates”. *Cement and Concrete Research*, V. 75, 2015, pp. 91–103.
17. De Weerdt, K., Ben Haha, M., Le Saout, G., Kjellsen, K. O., Justnes, H., and Lothenbach, B., “Hydration mechanisms of ternary Portland cements containing limestone powder and fly ash”. *Cement and Concrete Research*, V. 41, No. 3, 2011, pp. 279–291.
18. Deschner, F., Winnefeld, F., Lothenbach, B., Seufert, S., Schwesig, P., Dittrich, S., Goetz-Neunhoeffer, F., and Neubauer, J., “Hydration of Portland cement with high replacement by siliceous fly ash”. *Cement and Concrete Research*, V. 42, No. 10, 2012, pp. 1389–1400.
19. Duchesne, J., and Bérubé, M. A., “Effect of Supplementary Cementing Materials on the Composition of Cement Hydration Products”. *Advances in Cement Based Materials*, V. 2, 1995, pp. 43–54.
20. Deschner, F., Lothenbach, B., Winnefeld, F., and Neubauer, J., “Effect of temperature on the hydration of Portland cement blended with siliceous fly ash”. *Cement and Concrete Research*, V. 52, 2013, pp. 169–181.
21. Babaahmadi, A., Machner, A., Kunther, W., Figueira, J., Hemstad, P., and De Weerdt, K., “Chloride binding in Portland composite cements containing metakaolin and silica fume”. *Cement and Concrete Research*, V. 161, 2022, p. 106924.
22. Richardson, I. G., Skibsted, J., Black, L., and Kirkpatrick, R. J., “Characterisation of cement hydrate phases by TEM, NMR and Raman spectroscopy”. *Advances in Cement Research*, V. 22, No. 4, 2010, pp. 233–248.
23. Scrivener, K. L., Bazzoni, A., Mota, B., and Rossen, J. E., “Electron microscopy”. *A pratical guide to microstructural analysis of cementitious materials*, First issued in paperback, K. L. Scrivener, R. Snellings, and B. Lothenbach, eds., CRC Taylor & Francis, Boca Raton, 2017.
24. Münch, B., Martin, L., and Leemann, A., “Segmentation of elemental EDS maps by means of multiple clustering combined with phase identification”. *Journal of Microscopy*, V. 260, No. 3, 2015, pp. 411–426.
25. Georget, F., Wilson, W., and Scrivener, K. L., “edxia: Microstructure characterisation from quantified SEM-EDS hypermaps”. *Cement and Concrete Research*, V. 141, No. 10, 2021, p. 106327.
26. Chambolle, A., “An Algorithm for Total Variation Minimization and Applications”. *Journal of Mathematical Imaging and Vision*, V. 20, No. 1, 2004, pp. 89–97.
27. Georget, F., Schmatz, J., Wellmann, E., and Matschei, T., “A critical catalogue of SEM-EDS multispectral maps analysis methods and their application to hydrated cementitious materials”. *Journal of Microscopy*, V 294, No. 2, 2023, pp. 105-116.
28. Durdziński, P. T., Dunant, C. F., Haha, M. B., and Scrivener, K. L., “A new quantification method based on SEM-EDS to assess fly ash composition and study the reaction of its

individual components in hydrating cement paste". *Cement and Concrete Research*, V. 73, 2015, pp. 111–122.

APPENDIX A: ATOMIC RATIO DISTRIBUTIONS

Table 5: Numerical values for Ca/Si-ratio from map scan data, and 5th percentile from point scan data.

Ca/Si		PC-L			PC-FA			PC-VP	
Temperature	20°C	38°C	60°C	20°C	38°C	60°C	20°C	38°C	60°C
Mean value:	1.69	1.67	1.68	1.30	1.33	1.50	1.42	1.53	1.46
Std. dev. (sample):	0.73	0.70	0.64	0.49	0.49	0.63	0.62	0.64	0.63
95%:	3.10	3.03	2.91	2.23	2.26	2.72	2.63	2.78	2.69
75%:	2.08	2.05	2.02	1.53	1.56	1.83	1.73	1.87	1.78
Median:	1.55	1.55	1.57	1.19	1.23	1.38	1.29	1.41	1.33
25%*:	1.15	1.15	1.22	0.95	0.99	1.03	0.97	1.06	1.00
5%:	0.76	0.77	0.87	0.72	0.75	0.71	0.67	0.71	0.67
Point scans (5th %)	1.35	1.19	1.34	0.94	0.99	1.02	0.79	0.86	0.89

*: This percentile is used for comparison with the point scan method.

Table 6: Numerical values for Al/Ca-ratio from map scan data, and 50th percentile from point scan data.

Al/Ca		PC-L			PC-FA			PC-VP	
Temperature	20°C	38°C	60°C	20°C	38°C	60°C	20°C	38°C	60°C
Mean value:	0.28	0.29	0.23	0.30	0.30	0.34	0.33	0.34	0.34
Std. dev. (sample):	0.12	0.12	0.10	0.11	0.11	0.13	0.13	0.13	0.14
95%:	0.51	0.52	0.42	0.50	0.50	0.58	0.58	0.58	0.59
75%:	0.35	0.37	0.29	0.37	0.37	0.43	0.42	0.42	0.43
Median:	0.27	0.27	0.22	0.29	0.29	0.33	0.32	0.32	0.32
25%:	0.20	0.20	0.16	0.23	0.22	0.25	0.23	0.24	0.23
5%*:	0.13	0.13	0.11	0.15	0.15	0.16	0.15	0.15	0.14
Point scans (50th %)	0.06	0.06	0.07	0.14	0.17	0.15	0.13	0.13	0.13

*: This percentile is used for comparison with the point scan method.

Table 7: Numerical values for Al/Si-ratio from map scan data.

Al/Si		PC-L			PC-FA			PC-VP	
Temperature	20°C	38°C	60°C	20°C	38°C	60°C	20°C	38°C	60°C
Mean value:	0.45	0.45	0.38	0.37	0.38	0.48	0.44	0.48	0.46
Std. dev. (sample):	0.20	0.20	0.18	0.15	0.16	0.20	0.19	0.20	0.21
95%:	0.84	0.83	0.73	0.65	0.68	0.86	0.80	0.86	0.85
75%:	0.55	0.57	0.46	0.45	0.46	0.60	0.54	0.60	0.58
Median:	0.41	0.42	0.33	0.35	0.36	0.45	0.41	0.45	0.42
25%:	0.30	0.31	0.25	0.27	0.27	0.33	0.30	0.33	0.30
5%*:	0.19	0.20	0.17	0.19	0.19	0.21	0.19	0.21	0.18
Point scans (5th %)	0.05	0.07	0.08	0.12	0.15	0.15	0.10	0.11	0.11

*: This percentile is used for comparison with the point scan method.